of drag permits understanding the effect of different target particle sizes at the same bulk porosity and density, the effect of atmospheric density at the same atmospheric pressure, and the effect of atmospheric composition (viscosity). These results also suggest that both dynamic (d/g) and static ($P/\delta_t v^2$) pressures play roles. From equations (1) and (2) the combined roles yield the following alternative empirical expressions:

$$k\pi_2{}^{\alpha}\pi_v \sim f_0(P) f_e(P) \quad (17a)$$

$$k\pi_2{}^{\alpha}\pi_v = (P/\delta_t v^2)^{-\beta}(d/g)^{-\alpha} \quad (17b)$$

$$k\pi_2{}^{\alpha}\pi_v \equiv [(P/\delta_t v^2)^{\beta/\alpha}(d/g)]^{-\alpha} \quad (17c)$$

The same form of equation (17c) can be predicted from dimensional analysis with the additional constraint imposed by the coupling parameter:

$$k\pi_2{}^{\alpha}\pi_v \sim \{[(P/\delta_t v^2)\pi_2{}^{\alpha/3}]^{\beta'}(d/g)\}^{-\alpha}(\delta_p/\delta_t)^{\omega} \quad (18)$$

where a dependence on the projectile/target density ratio has now been included [see *Holsapple and Schmidt*, 1987]. If the role of atmospheric pressure replaces the effect of strength in equation (9), then the exponent $\beta'\alpha$ should be close to β. If β' is taken as 0.6 (see discussion with equation (9)) and α is about 0.5, then β should be about 0.3. The working value of 0.23 is slightly different and could reflect the additional roles of strength or some other competing process yet to be identified. Figure 10 combines the various data sets in order to test the idea that the appropriate pressure parameter involves dynamic as well as static processes explicitly expressed in equation (18). Adoption of a common value of β' is for simplicity and because it is unknown how the atmosphere might affect the coupling exponent μ discussed by *Holsapple and Schmidt* [1987]. Figure 10 reveals that the perspective provided by equation (18) allows understanding the response of very different target types over a wide range of atmospheric pressures and densities. Nevertheless, increased scatter in the data at higher velocities for denser gases suggests that either a changing drag coefficient at large Reynolds numbers or projectile-atmosphere interactions further affect crater scaling.

The effect of a changing drag coefficient can be explored by correcting for the various atmospheric effects and examining the data in terms of the Reynolds number. If the drag coefficient is assumed to be $24/Re$, then the data should exhibit relatively little scatter about a horizontal line. At higher Reynolds numbers, the drag coefficient will approach a

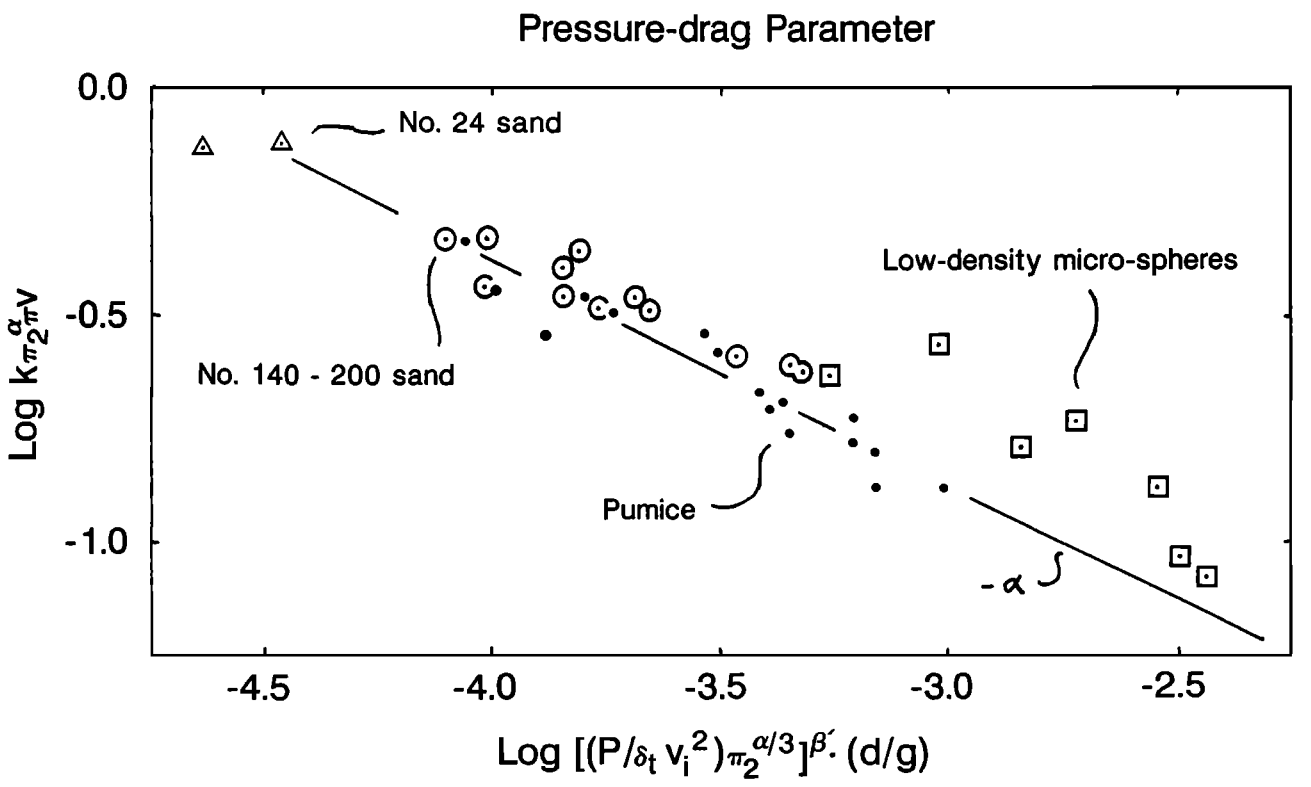

Fig. 10. Combined effects of atmospheric pressure and drag on cratering efficiency for different gravity-controlled particulate targets. The contrasting effects of an atmosphere on no. 24 and no. 140-200 sand can be understood in terms of the greater susceptibility of smaller ejecta particles to aerodynamic drag. The pressure parameter $(P/\delta_t v^2)\,\pi_2{}^{\alpha/3}$ is suggested by dimensional analysis (see equation (10d)). When dynamic pressure dominates growth, drag forces replace gravity forces in the π_2 parameter: hence the exponent should match $-\alpha$. When both static pressures and drag dominate scaling, the expected exponent ($-\alpha$) results in a pressure-dependent exponent $\beta'\alpha \sim -0.3$ close to the empirically derived value of 0.23 indicated in Figure 5a with $\beta' = 3\mu/2 = 0.6$, characteristic of particulate targets, where μ is the coupling parameter exponent from *Holsapple and Schmidt* [1987]. The slightly higher than expected values for microspheres most likely reflect a process of augmentation as found for no. 140-200 sand at higher densities (Figure 7b). All dimensions in cgs.